sustainability

MDPI

Article

Investigating the Effect of Parameters on Confinement Coefficient of Reinforced Concrete Using Development of Learning Machine Models

Gege Cheng [1], Sai Hin Lai [2,*], Ahmad Safuan A. Rashid [3], Dmitrii Vladimirovich Ulrikh [4] and Bin Wang [5]

[1] School of Teaching and Research Office, Yellow River Conservancy Technical Institute, Kaifeng 475004, China
[2] Department of Civil Engineering, Faculty of Engineering, Universiti Malaya, Kuala Lumpur 50603, Malaysia
[3] Faculty of Civil Engineering, Universiti Teknologi Malaysia, Johor Bahru 81310, Malaysia
[4] Department of Urban Planning, Engineering Networks and Systems, Institute of Architecture and Construction, South Ural State University, 76, Lenin Prospect, 454080 Chelyabinsk, Russia
[5] Henan New Development Construction Group Co., Ltd., Zhengzhou 450000, China
* Correspondence: laish@um.edu.my

Abstract: The current research aims to investigate the parameters' effect on the confinement coefficient, K_s, forecast using machine learning. Because various parameters affect the K_s, a new computational model has been developed to investigate this issue. Six parameters are among the effective parameters based on previous research. Therefore, according to the dimensions of the variables in the problem, a supply–demand-based optimization (SDO) model was developed. The performance of this model is directly dependent on its main parameters, such as market size and iteration. Then, to compare the performance of the SDO model, classical models, including particle swarm size (PSO), imperialism competitive algorithm (ICA), and genetic algorithm (GA), were used. Finally, the best-developed model used different parameters to check the uncertainty obtained. For the test results, the new SDO-ANFIS model was able to obtain values of 0.9449 and 0.134 for the coefficient of determination (R2), and root mean square error (RMSE), which performed better than other models. Due to the different relationships between the parameters, different designed conditions were considered and developed based on the hybrid model and, finally, the number of longitudinal bars and diameter of lateral ties were obtained as the strongest and weakest parameters based on the developed model for this study.

Keywords: prediction; confinement coefficient; supply–demand-based optimization; concrete technology

Citation: Cheng, G.; Lai, S.H.; Rashid, A.S.A.; Ulrikh, D.V.; Wang, B. Investigating the Effect of Parameters on Confinement Coefficient of Reinforced Concrete Using Development of Learning Machine Models. *Sustainability* **2023**, *15*, 199. https://doi.org/10.3390/su15010199

Academic Editors: Liborio Cavaleri, Ruben P. Borg and Panagiotis G. Asteris

Received: 25 October 2022
Revised: 9 December 2022
Accepted: 16 December 2022
Published: 22 December 2022

1. Introduction

Design procedures for reinforced concrete (R/C) structures often require ductile behavior. The ductile behavior can be provided by confining the concrete with the lateral or spiral reinforcement [1]. By implementing lateral or spiral reinforcements, the strength and ductility in the R/C increase significantly. In order to increase the strength of R/C columns, the confinement coefficient, K_s, can be used. Over the past few years, many studies have been conducted to predict the confinement degree. In the proposed models, various conditions and parameters have been considered for confined concrete. Considering the concrete confined by rectangular steel hoops, Ken and Park [2] presented a stress–strain diagram. This diagram consists of three parts, including a parabola to the maximum stress point, a strongly descending linear section, and a horizontal linear section. In the horizontal section, the stress is constant and equal to 0.2 of the maximum stress. In the descending portion of the diagram, factors such as concrete cylinder strength, the width of confined concrete to the hoops distance ratio, and the ratio of hoops volume to the concrete core volume affect the line slope. Park et al. [3] developed the diagram designed by Kent and

Park [2] and improved it. Sheikh and Uzumeri [4] provided 24 short tied columns and put them under uniform axial pressure. Their main purpose of executing these experiments was to analyze the effect of different parameters on the behavior of tied columns. They stated that the most important effective factors include the tie configuration, distribution of longitudinal steel, column perimeter, longitudinal column steel, and the rate of lateral confinement. In addition, Sheikh and Uzumeri [5] proposed a stress–strain curve according to the finding of their experiments conducted on confined concrete. They concluded that the concrete strength and ductility increased as a result of the reduced tie spacing and distribution of longitudinal steel. Considering the confined concrete, Saatcioglu and Razvi [6,7] highlighted a stress–strain diagram. This diagram consists of two sections: an ascending part in the form of a parabola and a linear descending part. In the descending portion of the curve, the strain is equal to 85% of the peak stress. In another part of the diagram, a constant residual strength at the strength level of 20% has been considered. Though the above mentioned model is an analytical model, its parameters were obtained using a large quantity of experimental data. These experimental data are related to concretes where some of them have been well confined and some have been poorly confined. Additionally, in order to assess the performance of the above mentioned model, its results were compared with the results of a large number of concrete columns. According to an experimental study conducted on 65 concrete columns, Chung et al. [8] stated a strain–stress relationship. The parameters affecting this model include the concrete strength, volume ratio, confinement type of rectilinear ties, and distribution of longitudinal.

Using neural network modeling, the above mentioned behavioral models can be validated. Therefore, by the use of the experimental model proposed by Chung et al. [8], a neural network model was trained and tested. Over recent years, the use of a neural network, which is able to obtain a high level of accuracy for non-linear problems, has significantly increased [9–14]. The most important advantages of a neural network are as follows:

The neural network is developed based on experimental data, and this way, it can present appropriate solutions for different problems. New techniques have been developed to solve problems with large and complex data, based on intelligent models and metaheuristic algorithms. Various applications of these models have been highlighted in civil, mining, and petroleum engineering [15–45]. However, algorithms based on artificial neural networks (ANN), decision trees, hybrids, adaptive neuro-fuzzy inference system (ANFIS) models, among others, are recent examples of predictive models that are developing and increasing efficiency in different engineering fields [39,46]. Optimization algorithms such as particle swarm optimization (PSO), firefly algorithm, imperialism competitive algorithm (ICA), genetic algorithm (GA), etc., are used in the development of forecasting models [47–62]. Over time and by changing the conditions, neural networks can cover these changes and match solutions. Using a neural network, theoretical, experimental, empirical data, or a combination of them, can be analyzed effectively and with sufficient accuracy [63].

In the current research, a hybrid ANFIS model was developed in order to estimate K_s in the R/C rectangular columns. This was executed in order to maximize accuracy. When previous research was taken into consideration, it is possible to draw the conclusion that the K_s prediction is fraught with unpredictability because of the many different parameters. As a result, there is a requirement for the development of a new model that, in addition to providing accurate forecasts, is able to evaluate the impact of various parameters. The primary objective of this study is to develop a novel hybrid-ANFIS method for predicting K_s. This novel algorithm, which is based on supply–demand-based optimization (SDO), will be presented as a new hybrid approach in this work. After that, its effectiveness is analyzed with the help of traditional models. Lastly, the uncertainty effect caused by the parameters is taken into account by the superior model.

2. Experimental Setting

2.1. Data

Conducting an experimental study on 65 concrete columns, Chung et al. [8] presented a strain–stress relation for confined concrete, and this way, they investigated the effect of confinement by lateral tie on the concrete columns. They considered the cross sectional area of the columns, concrete cover thickness, and longitudinal reinforced diameter, to be 600 mm, 17 mm, and 12 mm, respectively. The letters L, M, and H show the compressive strength of 20, 39, and 34 MPa for concrete, respectively (Figure 1). The letter P also shows the plain concrete column which has no bars. In order to develop a neural network, the experimental studies conducted by Chung et al. [7] were used. Some of the data related to their studies used for neural network modeling are shown in Table 1. These data include compressive strength of concrete (f'_c), yield strength of lateral tie f_{yh}, number of longitudinal bars (m), spacing between lateral ties (s), diameter of lateral ties φ_h, volumetric ratio of lateral ties ρ_s, and lateral confinement coefficient K_s.

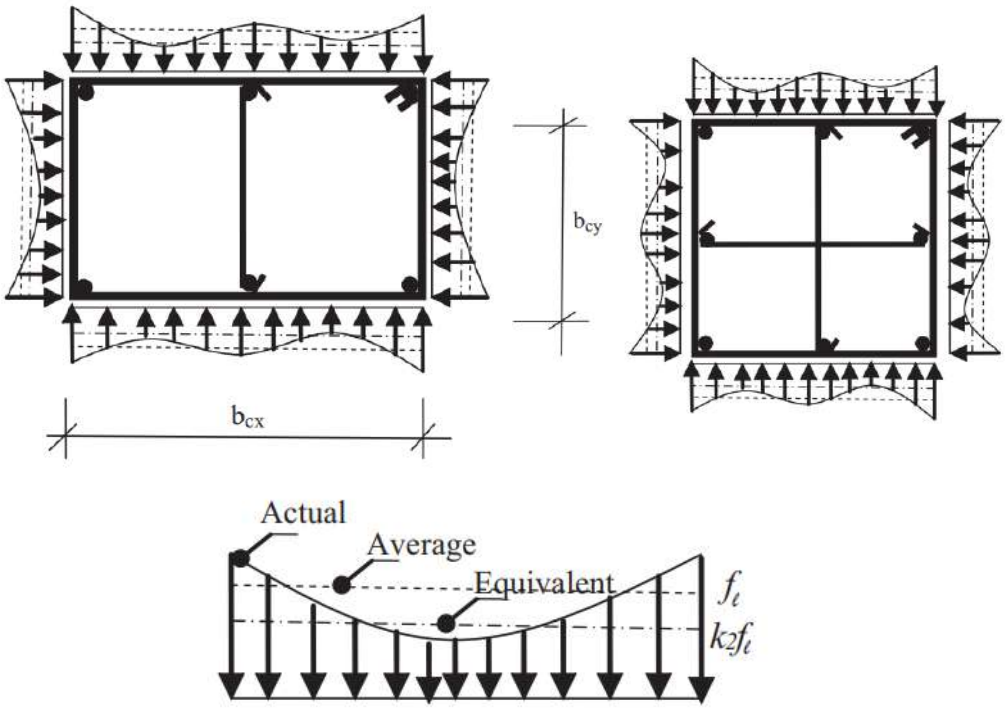

Figure 1. Characteristics of the designed cases.

Table 1. The information of the designed model.

Parameter	X1	X2	X3	X4	X5	X6	Y
Symbol	m	φ_h	f'_c	ρ_s	f_{yh}	s	K_s
Limit	8–12	6–8	19.6–56.4	0.007–0.051	550–1300	30–100	0.81–3.6
Unit	-	mm	MPa	-	MPa	mm	-

2.2. Previous Analytical Models

In order to assess the increased strength of R/C columns, the confinement coefficient, K_s can be used. Over the past few years, many studies were used to predict the confinement degree. In the proposed models, different conditions and parameters affecting confined concrete were considered [4,6,8,64]. In the following, the studies conducted to predict lateral confinement coefficient are presented:

Park et al. [64] modified the stress–strain relation in confined concrete and obtained a new relation for passive confinement. The K_s coefficient controlled this new relation. Of course, in their studies, the effect of two parameters of lateral reinforcement arrangements and the location of longitudinal reinforcement were not applied. The above mentioned relation was obtained as follows:

$$K_s = 1 + \frac{\rho_s f_{yh}}{f'_c} \tag{1}$$

where ρ_s was obtained as follows:

$$\rho_s = \frac{A_{sh} l_s}{s b'_c d'_c} \tag{2}$$

In relation (2), the width and depth of the confined core (which are measured up to the external part of ties) are shown by b'_c and d'_c, respectively. The ties center-to-center distance and the total length of lateral ties are shown by S and l_s, respectively.

Sheikh and Uzumeri [4] conducted an experimental study on the stress–strain relation. They supposed that the K_s parameter is affected by the increased strength of the concrete. An increase in the strength also occurred as a result of the concrete rectilinear reinforcement. Additionally, they applied the effect of rectilinear reinforcement in the form of square root of volumetric ratio. Using regression analysis, K_s parameter was obtained as follows:

$$K_s = 1 + \frac{b_c^2}{140 P_{occ}} \left[\left(1 - \frac{m c_i^2}{5.5 b_c^2}\right) \left(1 - \frac{s}{2 b_c}\right)^2 \right] \sqrt{\rho_s f_{yh}} \tag{3}$$

$$P_{occ} = 0.85 f'_c (A_{ck} - A_{st}) \tag{4}$$

In relations (3) and (4), the parameters A_{st}, A_{ck}, c_i, and m indicate the area of total longitudinal reinforcement. The volumetric ratio of the lateral ties' parameter is also obtained as follows:

$$\rho_s = \frac{A_{sh} l_s}{s b_c d_c} \tag{5}$$

where the width and depth of the confined core (which is measured up to the center of ties) are shown by b_c, and d_c, respectively.

Based on their research studies, Saatcioglu and Razvi [6] concluded that passive lateral pressure was not always uniform. Therefore, the above-mentioned model was built based on the equivalent uniform pressure calculation. Actually, the effect of this pressure is similar to non-uniform confinement pressures which are created in different columns. These columns may be strengthened in different orders and structures (Figure 1). The relation related to K_s calculation is as follows:

$$k_s = 1 + \frac{6.7}{f'_c} (f_{1e})^{-0.17} f_{1e} \tag{6}$$

In order to calculate the equivalent uniform pressure f_{1e}, in relation (6), the following relation was used:

$$f_{1e} = k_2 f_1 = k_2 \frac{\sum A_{sh} f_{yh} sin\alpha}{s b_c} \tag{7}$$

In relation (7), the medium lateral pressure and the angle between transverse reinforcement and b_c are shown by f_1 and α, respectively. The K_2 coefficient defined to decrease the average pressure is also shown as follows:

$$k_2 = 0.26 \sqrt{\left(\frac{b_c}{s}\right)\left(\frac{b_c}{c_i}\right)\left(\frac{1}{f_1}\right)} \leq 1 \tag{8}$$

3. Methodology

The present methodology explains the inspiration of supply–demand-based optimization (SDO); afterwards, it provides the detailed mathematical model of SDO.

3.1. Inspiration

Based on the economic theory, within a given market, first, the commodity quantity (CQ) and commodity price (CP) may be exposed to various fluctuations; then, they may be progressively stable onto their corresponding points of equilibrium [65]. In general, this procedure is dependent upon both the producers' supply relation and the consumers' demand relation [66]. In a market economy, there is an economic theory which called the supply–demand mechanism (SDM) for determining the price. Based on this theory, the CQ in the next time q_{t+1}, with considering its current price p_t. within a market is specified by taking into account the producers' supply relation, that is $q_{t+1} = f(p_t)$, where f stands for a linear supply function. In a given market, with the rise of the current CP, the CQ rises in supply at the next time [66]. With the rise in the commodity quantity, its price reduces; thus, g will be a reducing function. When oscillation occurs, the two functions will be intersected eventually at a certain point P(x0, y0), called the equilibrium point, where x0 and y0. Equation (9) expresses the supply function f [66] as follows:

$$q_{t+1} - q_0 = a(p_0 - p_0) \tag{9}$$

On the other hand, Equation (10) expresses the demand function g [61] as follows:

$$p_{t+1} - p_0 = -b(q_{t+1} - q_0) \tag{10}$$

where t stands for the time, a and b represent the linear coefficients. In general, the SDM is in two different modes: stability and instability, as can be observed in Figure 2A,B, respectively. In case $|ab| < 1$, the supply function f will be steeper compared to the demand function g; the extent of oscillations then decreases at each time. Thus, the CP and quantity curve tends to spiral inwards with respect to time. As a result, with time passing, the price and quantity will diverge from the point of equilibrium (x0, y0) progressively [65]. The cobweb model is a popular theory in the economic context based on which fluctuation in price will lead to fluctuation in supply, thereby resulting in a sporadic rise or fall of price. As a result, this model has been widely applied to investigating the price fluctuations of different products in given markets.

3.2. Developing SDO

Based on the SDM, the stability mode is capable of encouraging both the CP and CQ to exploit the equilibrium-point neighborhood, and such an exploitation process oscillates in magnitude over time. However, the instability mode typically forces both the CP and CQ to progressively find new areas positioned far from the point of equilibrium. The stability mode that is slowly reducing the oscillations in the SDM is able to be simply introduced to SDO as exploitation to carry out a local search within an encouraging area. Likewise, it is also possible to lend the instability mode to SDO as exploration in such a way as to carry out a search globally within the search space. Figure 3 demonstrates converting the SDM condition to the SDO algorithm. In case this solution outperforms the candidate solution, it will be used instead of the candidate one. It is worth mentioning that the method introduced in this study is actually an algorithm that works based on a swarm optimization; as a consequence, two matrixes are provided to present the CP and commodity quantity, respectively.

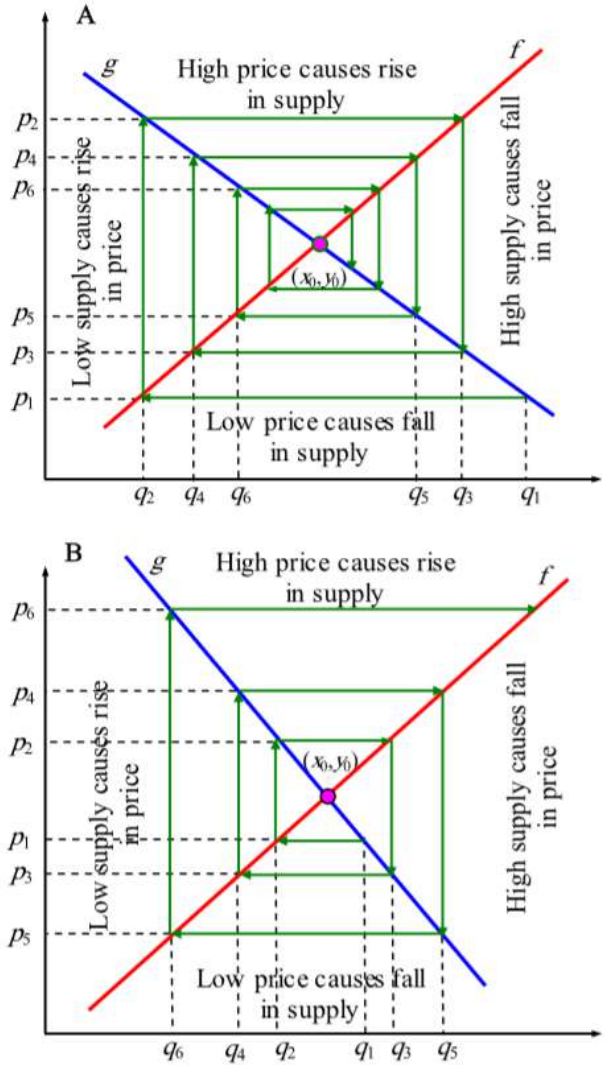

Figure 2. The (**A**) stability (**B**) instability modes of SD condition.

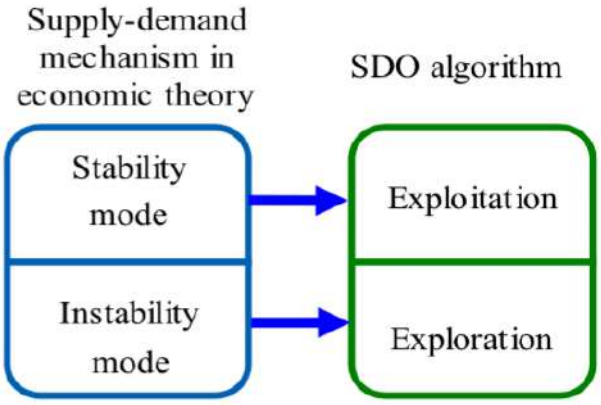

Figure 3. Converting the SDM condition to the SDO algorithm.

In case the variable L equals the product of α (supply weight) and β (demand weight), the following relation will be achieved:

$$L = \alpha\beta = \frac{4.(T - t + 1)}{T}.\sin(2\pi r).\cos(2\pi r) \quad (11)$$

If $|L| < 1$ corresponds to the stability mode as displayed in Figure 4A, various CP vectors around the equilibrium price x0 are achieved considering the current price vector through the adjustment of the weights α and β. In this case, we can indicate that with the help of this algorithm, each market will be capable of updating all of its CPs in the neighborhood of the current CPs and mimicking the stability mode depicted in Figure 2A. Such a mechanism puts a focus on exploitation and gives the SDO algorithm encouragement for searching at a local level. As can be observed in Figure 4B, $|L| > 1$ corresponds to the instability mode, which makes the CP vector within any market capable of moving to make a simulation of the instability mode displayed in Figure 2B. Such a mechanism is concentrated upon exploration, and because of this mechanism, SDO has to perform a global search.

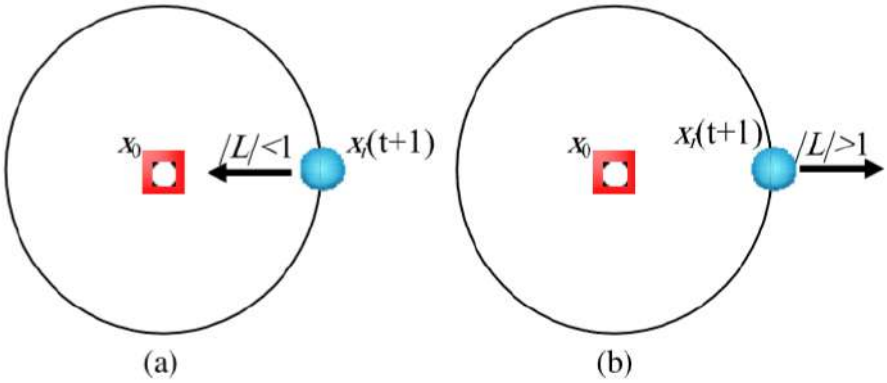

Figure 4. The two modes of SDO (**a**) stability; (**b**) instability.

Figure 5 displays the values of the variable L over iterations, where T is fixed at 1000. As the figure demonstrates, in the initial iterations, the L values are $L > 1$ or $L < -1$ with a high probability. With the rise of the iterations, such high probability starts to drop, and an increasing probability exists, indicating that the L function values are in the interval of $[-1, 1]$. In the following iterations, the L values are in the interval of $[-1, 1]$ with an increasingly high probability. It is obvious that in the primary stage of iterations, SDO achieves high exploration and then switches smoothly to high exploitation.

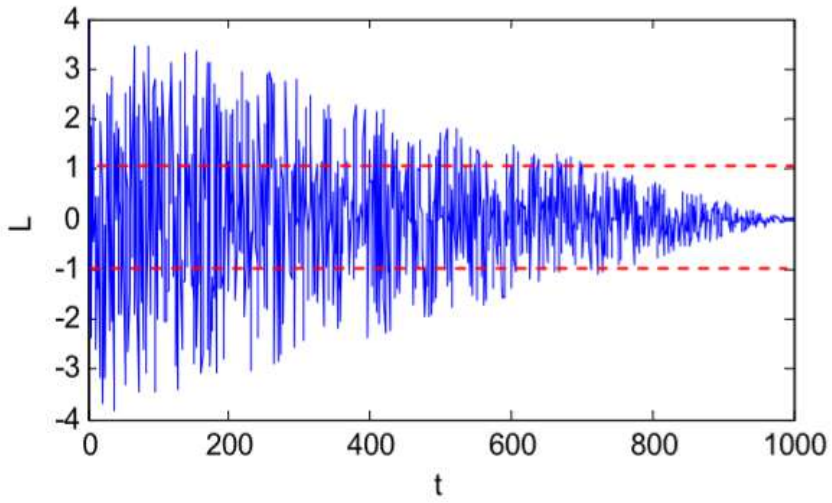

Figure 5. The distribution of the L parameter.

When both the CP and CQ vectors get updated in each iteration, they are assessed using their corresponding arrays. In case the fitness value of the ith CQ vector is better than

the fitness value of the ith CP vector, the ith CP vector is changed with this quantity vector as a chosen solution. The mechanism of this solution replacement is depicted in Figure 6.

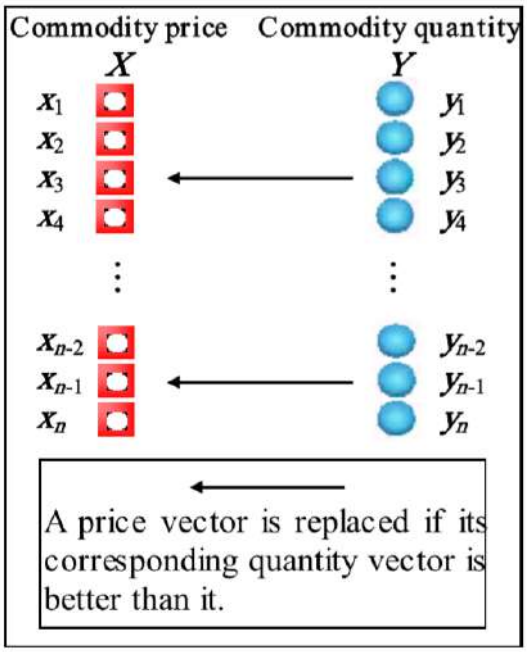

Figure 6. The plan of replacement for commodity.

The optimization process is started by SDO through forming a set of markets in a random way. At each iteration of this process, both the equilibrium quantity and the equilibrium price are taken into consideration to update each CQ of a market. After that, the equilibrium price is considered to update each CP of a market. It is possible to switch the equilibrium price vector in a random way between a selected CP vector from the price array on the basis of CP vectors. The CPs and CQs are updated in this way through the adjustment of the weights' values of both α and β. For the purpose of performing either exploration or exploitation, the L values are reduced linearly with a random fluctuation. The CPs of a market are inclined with the aim of diverging from the equilibrium price in cases where $|L| > 1$, while they converge toward the equilibrium price in the case where $|L| < 1$. Afterwards, the fitness function is employed in order to assess the updated price vectors and quantity vectors. For every market, when the fitness value of its CQs is better than the fitness value of its CPs, its commodity quantities are used instead of its CPs as a candidate solution. Finally, once the termination criterion is met, the optimum CP vector of a market is returned as the optimal solution explored.

4. Simulation Procedure

4.1. Pre-Training

The input variables are the most important factor affecting the accuracy of a computing model. In order to predict K_s (model output) in the RC columns, six parameters were considered in the input layer of the neural network. Based on the experimental studies conducted in the past years [67–69], the above mentioned six parameters were selected as the most important factors affecting K_s. The value variation range of these parameters is shown in Table 1. In order to compute the model, a total of 59 pieces of data were used, and their details are given in Table 1. The above mentioned 59 pieces of data (including K_s and the six parameters affecting them) were divided into two groups. Among them, the first 48 cases were considered for the training of the network (training data). The other ones, including the remaining data, were used to assess the neural network performance (testing data). In fact, 20% of the whole data, including 11 pieces of data that were selected randomly,

were considered to test the model in each training stage. In order to investigate the pre-training of the main models, an analysis was implemented on different combinations of data to evaluate the K_s parameter. Table 2 shows the main combinations of these data for designing computational models. This analysis helps to investigate the effect of parameters on the model structure and its performance in predicting the K_s parameter at each stage. Figure 7 shows the results of this analysis in which the least error is related to the G14.

Table 2. The main combinations of data.

Group	X1	X2	X3	X4	X5	X6	Y
G1	•		•		•		•
G2		•	•		•		•
G3			•		•	•	•
G4			•	•	•		•
G5	•	•	•		•		•
G6	•		•		•	•	•
G7	•		•	•	•		•
G8		•	•		•	•	•
G9		•	•	•	•		•
G10			•	•	•	•	•
G11	•	•	•		•	•	•
G12	•			•	•	•	•
G13		•	•	•	•	•	•
G14	•	•	•	•	•	•	•

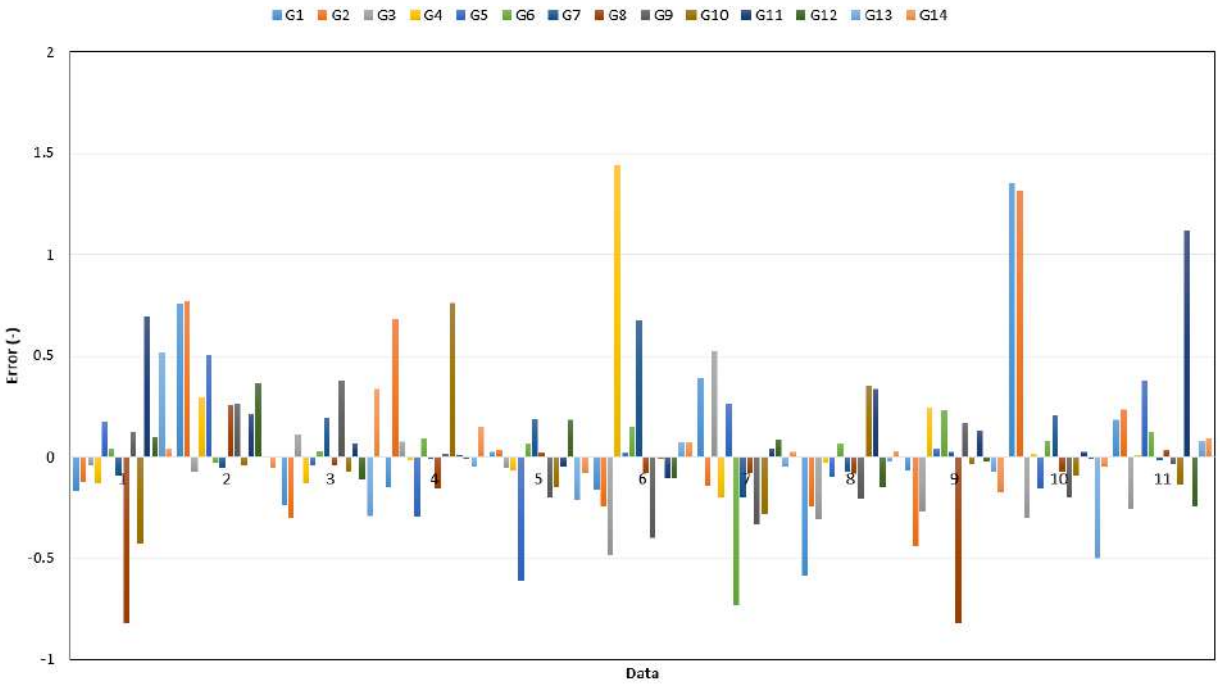

Figure 7. The 14 selected combinations to analyze the effect of parameters on output.

4.2. ANFIS

The ANFIS base structure is based on an extended fuzzy inference system (FIS)-based model. For better implementation of the structure, the ANFIS model uses the BP learning method. This method allows the membership function (MF) parameters of the FIS to develop different stages based on conditional rules ("if–then") [70]. These laws, which are based on the theory of Takagi and Sugeno fuzzy type, include different elements such as the middle layers, input, and output layers that are mentioned in Figure 8.

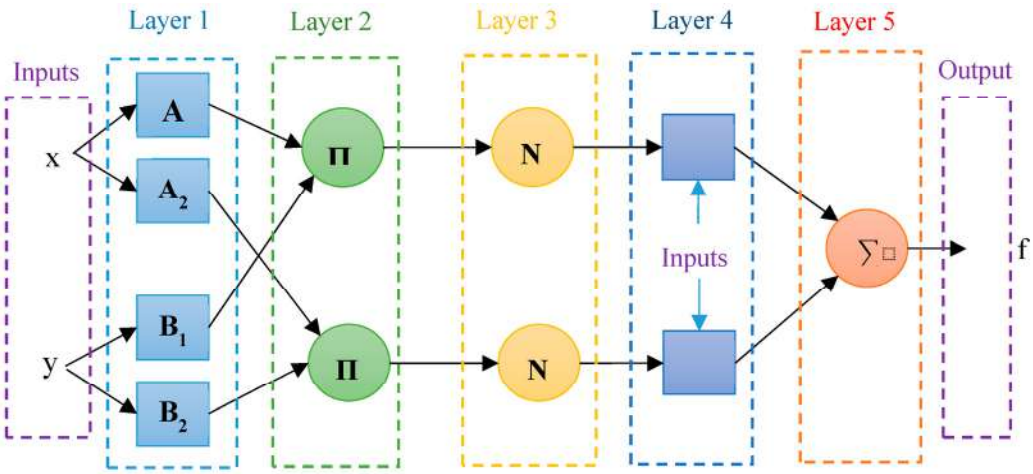

Figure 8. A view of the ANFIS structure.

The ANFIS structure in this research is developed and implemented from the BP algorithm based on the gradient descent (steepest descent) approach and finally, it is implemented to predict the K_s parameter. In the first step, the various parameters of the ANFIS model are determined for the optimal design of its structure based on previous research. With trial and error methods, the process continues until the best conditions are obtained. The results of the initial structure are presented in Table 3. Due to the existing conditions, the gradient descent method sometimes gets stuck in local minima, and optimization methods are used to solve this problem or to reduce it, to achieve more favorable results. Therefore, the model structure of this section is designed and developed based on two optimization algorithms in order to improve the performance of prediction models for K_s parameters.

Table 3. The performance of initial ANFIS and its optimum structure.

Parameters	Input MF Type	No. of Nonlinear Parameters	No. of MFs for Each Input	No. of Fuzzy Rules	No. of Linear Parameters	Output MF Type	No. of Output MFs	R^2 Training	R^2 Testing
Specification	Gaussian	100	6	8	100	Linear	8	0.8961	0.8821

4.3. SDO-ANFIS

According to the structure of the SDO optimization algorithm, the algorithm can provide suitable solutions for the problem by using two steps of searching and extracting the answer. According to this solution, a hybrid method between the optimization algorithm and the basic model called SDO-ANFIS was developed in this research. This new combination can prevent the model from getting stuck in local minima and determine the best structure minima. In addition, the SDO algorithm has wider capabilities and simpler parameters that can achieve the optimal conditions of the problem. This search process comes with the help of the ANFIS base model. By improving the performance of ANFIS functions, the performance of models for K_s prediction increases. In other words, the higher the power of the optimization algorithm in this new combination, the more accurate the optimal structure will be. In the following, more details about parameters of the SDO

algorithm are discussed and implemented to finalize the structure with higher accuracy and less error.

In this section, three other types of classical algorithms are used to evaluate the performance of the new SDO-ANFIS hybrid model. These algorithms, which include GA, PSO, and ICA, are examined under different conditions to provide the best assessment to solve the iron price-prediction problem. The two key parameters for the SDO algorithm are the number of iterations and the market size. Due to the fact that each algorithm has different functions in different conditions, the best mode is provided by trial and error method and design of different models. In Table 4, the results of the models in the optimal state of their coefficients are obtained. In all models, the number of iteration was considered to be 400.

Table 4. Prediction values of K_s using various hybrid-ANFIS Models.

Hybrid Models	Train		Test		Key Parameters	Coefficient Values
	R^2	RMSE	R^2	RMSE		
GA-ANFIS	0.9341	0. 129	0.9183	0.172	Iteration (Generation) = 400 Population size = 40	Crossover rate = 0.75 Mutation rate = 0.25
PSO-ANFIS	0.9229	0.144	0.9019	0.206	Iteration = 400 Swarm size = 35	Inertia coefficient = 0.75 Acceleration coefficients c1 = 2 and c2 = 2
ICA-ANFIS	0.9302	0.132	0.9217	0.154	Iteration (Ndecade) = 400 Ncountry = 30 Nimp = 10	-
SDO-ANFIS	0.9501	0.126	0.9449	0.134	Iteration = 400 Market size = 35	-

The results of Table 4 indicate that the performance of hybrid models is acceptable, and they can make a good assessment of the K_s. The new SDO-ANFIS model offers better results than other hybrid models. This high capability represents a successful new model for problem solving. Given this, it can be noted that the SDO-ANFIS model for training and testing data shows high flexibility. The results of all hybrid models are given in Figures 9–16.

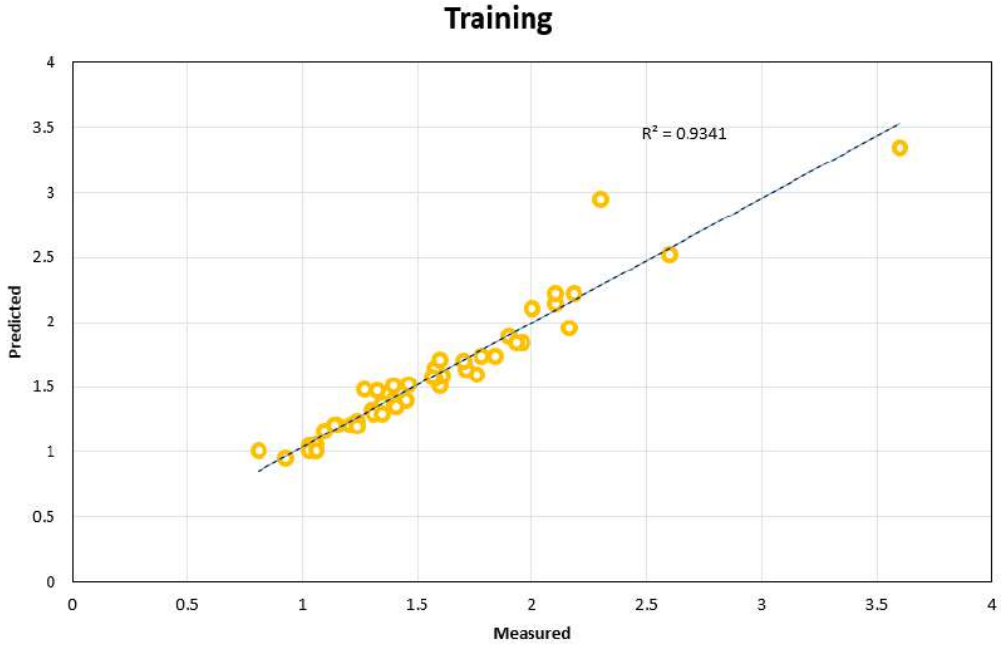

Figure 9. The result of GA-ANFIS model for training data.

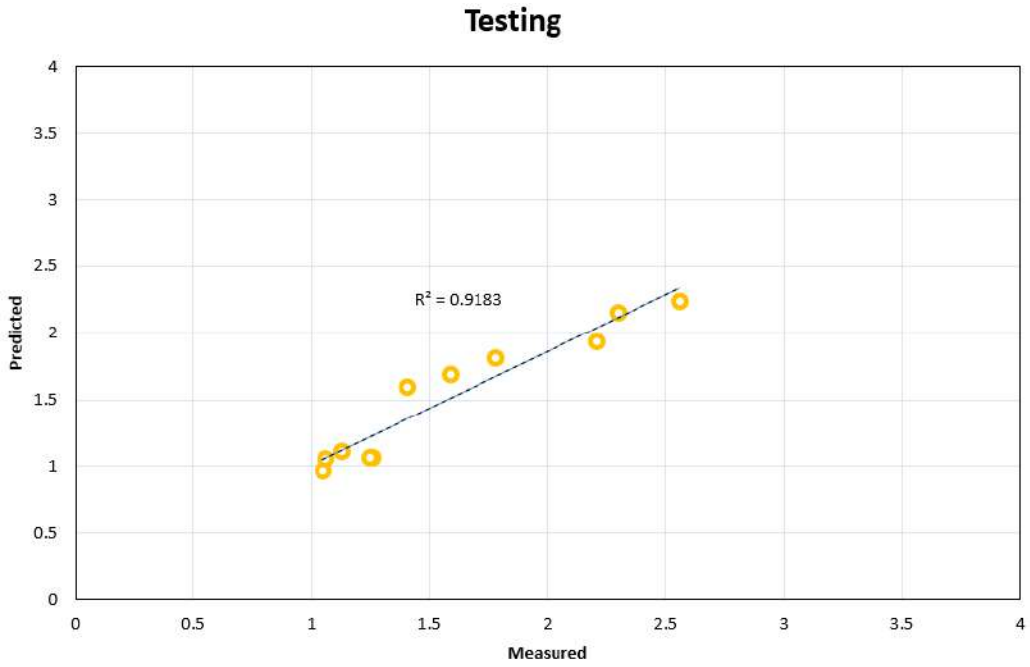

Figure 10. The result of GA-ANFIS model for testing data.

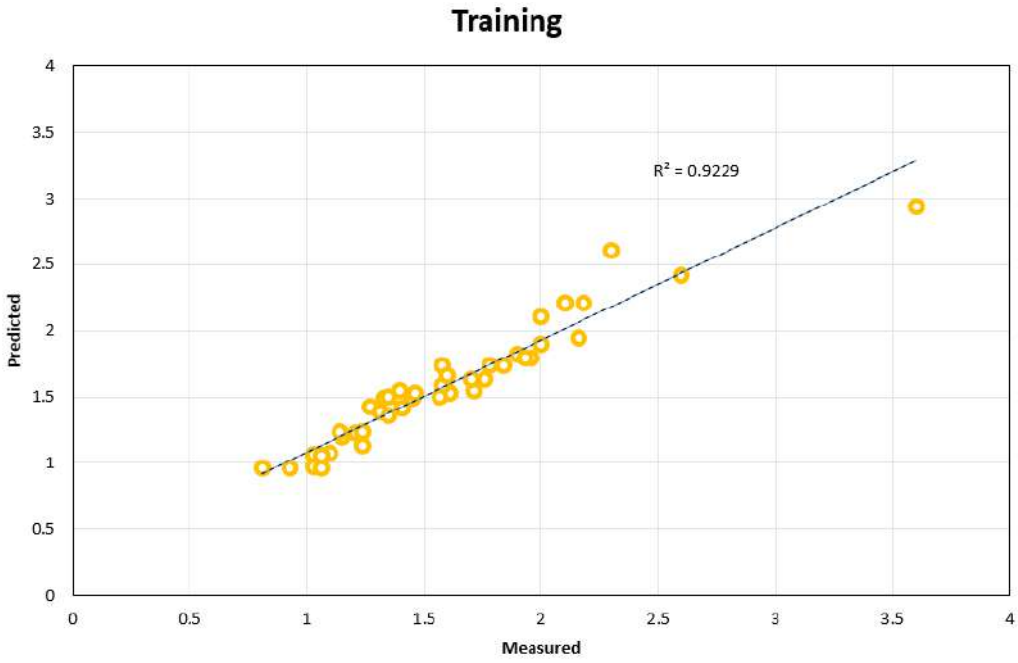

Figure 11. The result of PSO-ANFIS model for training data.

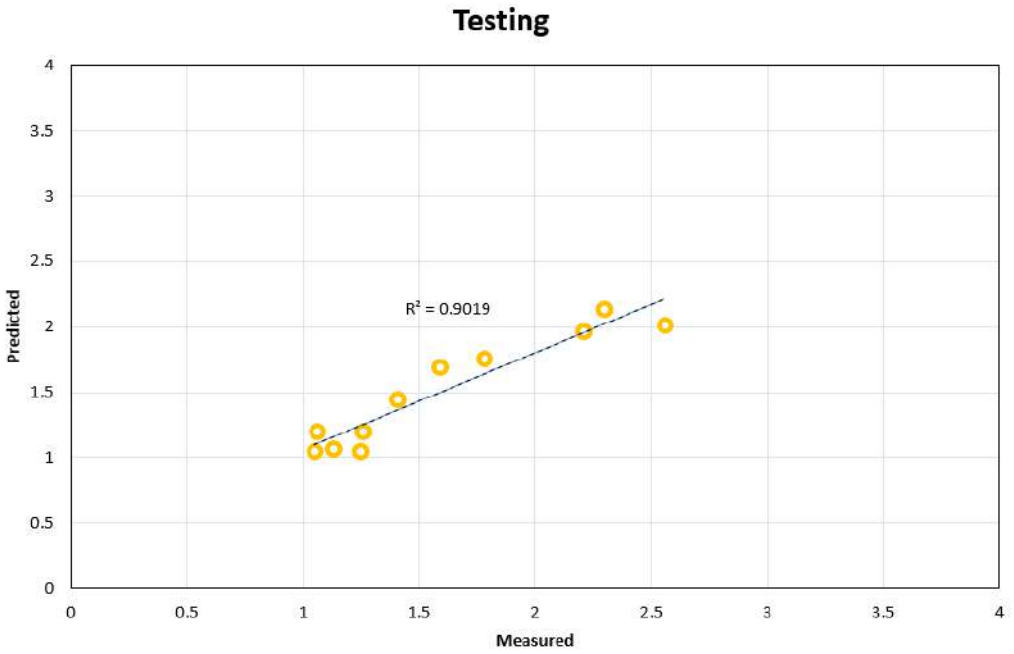

Figure 12. The result of PSO-ANFIS model for testing data.

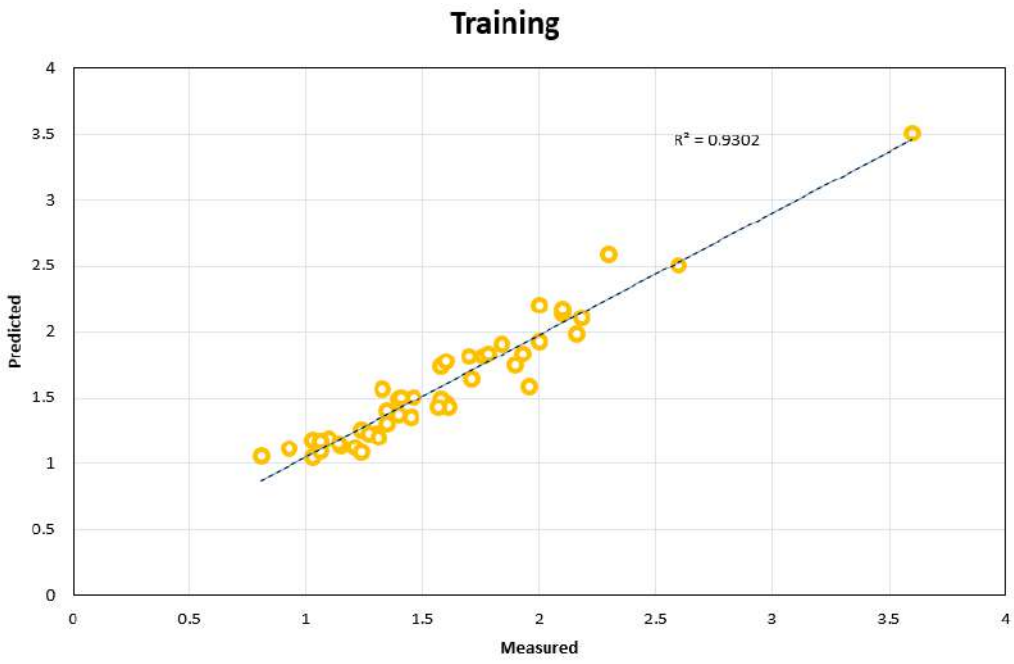

Figure 13. The result of ICA-ANFIS model for training data.

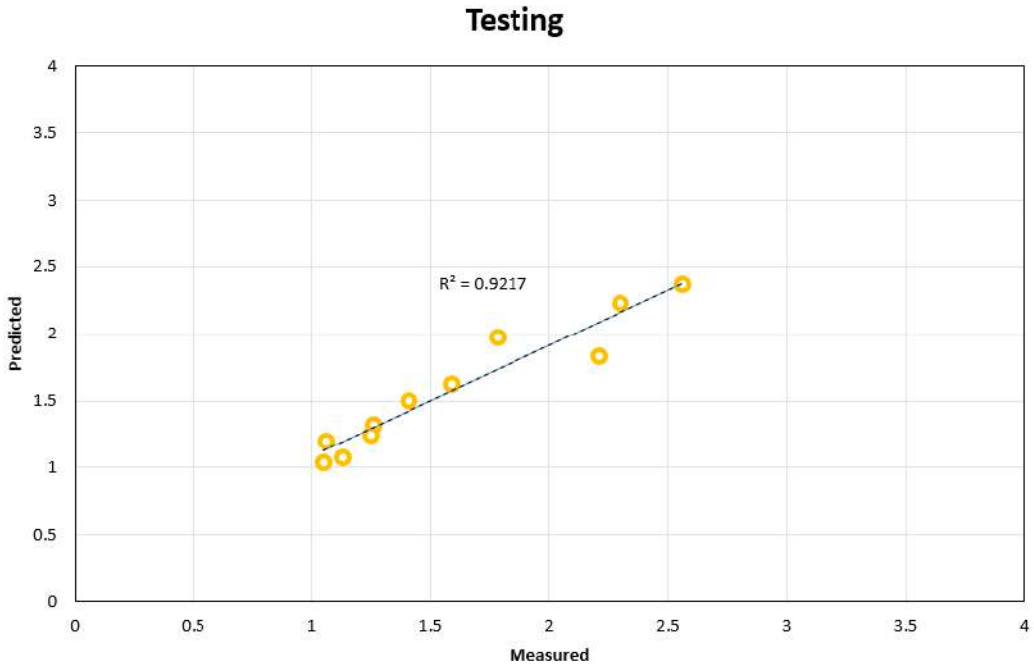

Figure 14. The result of ICA-ANFIS model for testing data.

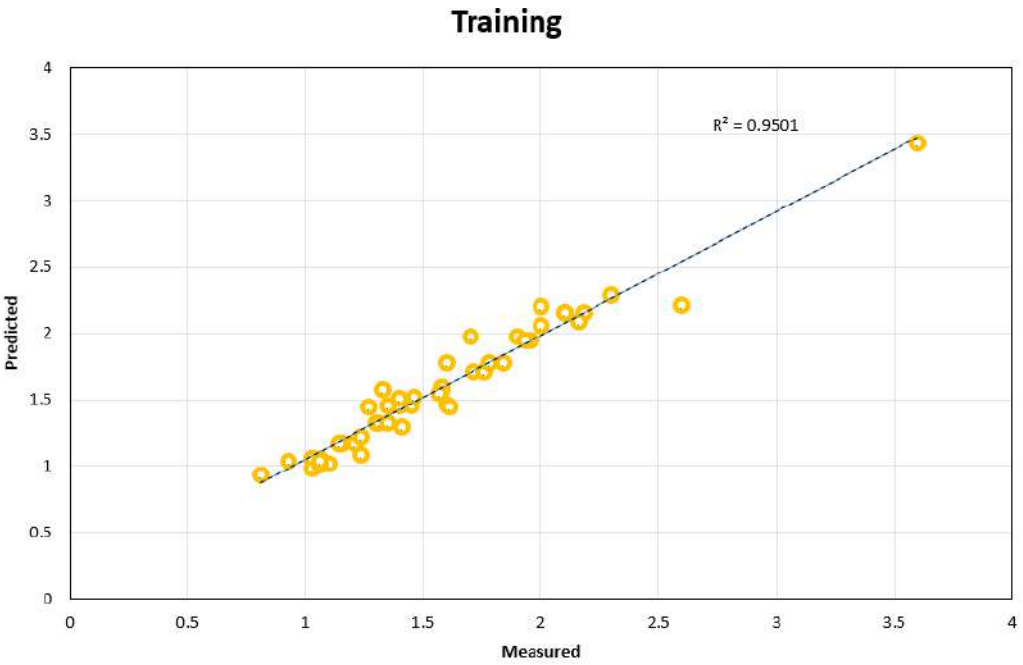

Figure 15. The result of SDO-ANFIS model for training data.

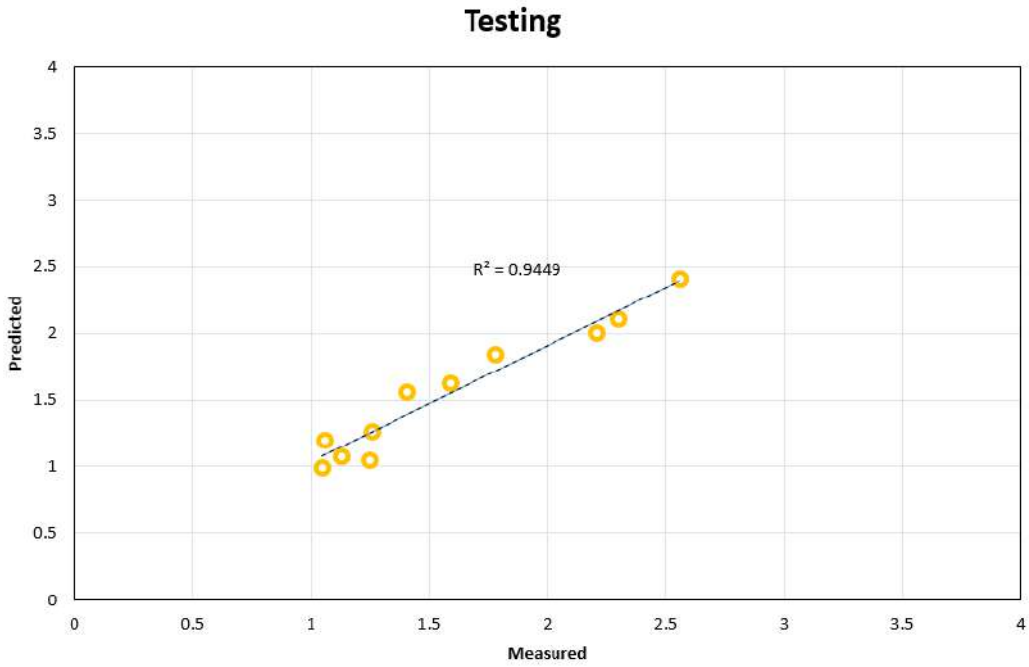

Figure 16. The result of SDO-ANFIS model for testing data.

5. Results and Discussion

The effect of the parameters in determining the K_s is one of the most important parts of this area. In order to investigate the effect of each of the input parameters on the network output, the sensitivity analysis was used. The sensitivity analysis allows for making the network smaller by removing the less effective and unimportant inputs. Given that interactions are seen in the data, it is impossible to determine each effect in the ordinary way. Therefore, in this section, using the superior model of the previous step (SDO-ANFIS), the effect of these parameters on and their uncertainty that have a final result are discussed. Figure 17 shows the effect of 6 parameters on the K_s. As can be seen, these parameters are one of the most important indicators affecting the K_s, and different effects cause uncertainty in them. The best parameter that has the most impact on the K_s is the X2 (φ_h) parameter while X1 (m) was the least effective parameter (0.2). In real conditions, the fyh (X5) parameter strongly affects K_s. However, as in this research only four different values of fyh, i.e., 500 MPa, 550 MPa, 900 MPa, and 1300 MPa, are considered to construct SDO-ANFIS, fyh showed a small effect. These parameters, because there are interdependencies between them, make it impossible to provide an accurate percentage. Therefore, the developed SDO-ANFIS model is used to check the uncertainty of the parameters. These results also show that due to the different uncertainties between the parameters, the best case should be determined based on important indicators.

Finally, a comparison between the results of the testing data using the four hybrid models is presented in Figure 18. In this figure, the difference between actual and predicted data is given. According to this figure, in four of the models, the least error belonged to the SDO-ANFIS model. In addition, as can be seen, the difference between the actual and predictive data in the SDO-ANFIS model is a definite range, while in other models, the results are seen with more discrepancies. This confirms that the model developed in this research has a lower error rate and can predict the K_s parameter more reliably than other models.

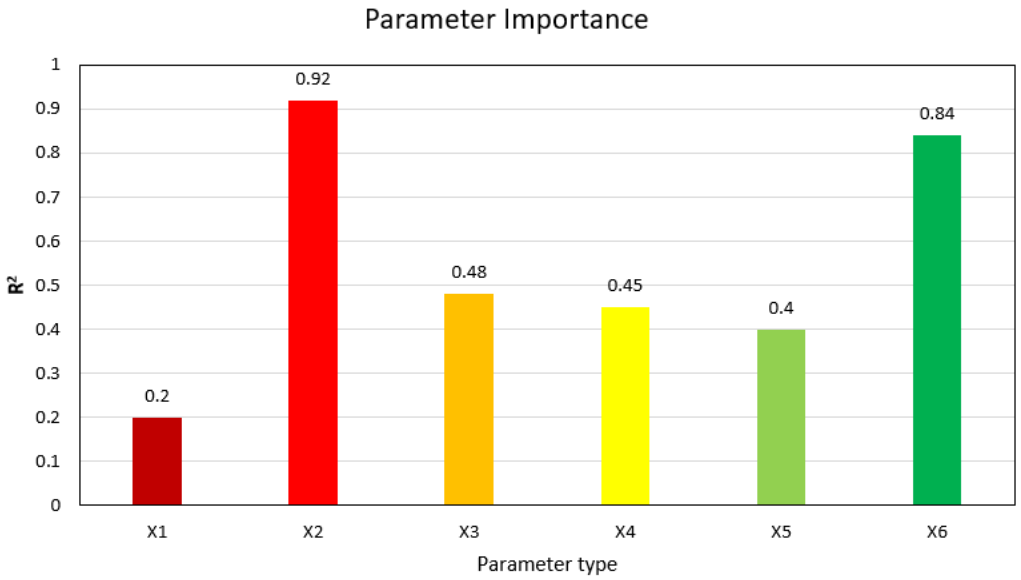

Figure 17. Influence of parameters on K_s.

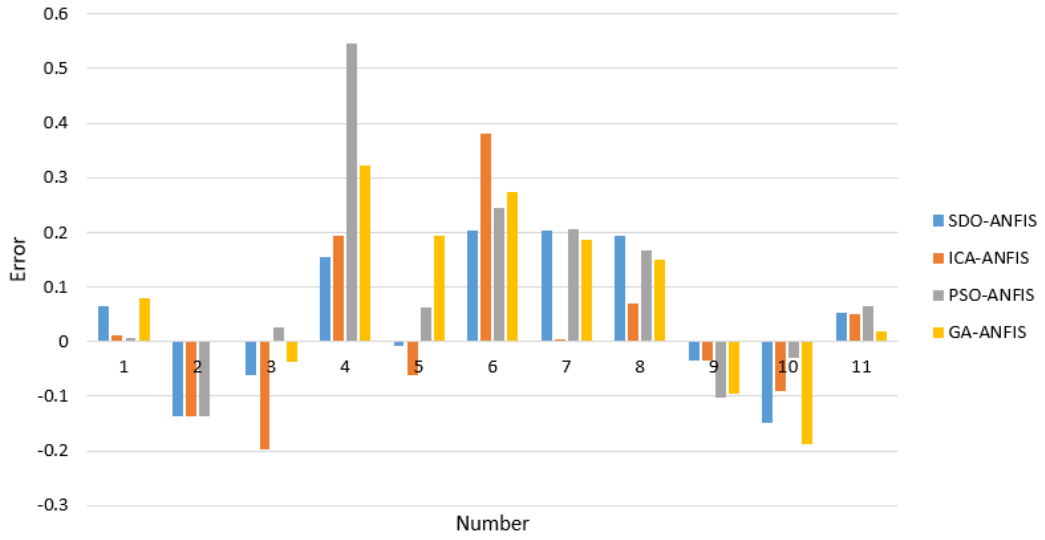

Figure 18. The difference between actual and predicted data.

6. Conclusions

In this study, using artificial intelligence models, the K_s was estimated. Due to the importance of this issue, the main and influential factors for the design of intelligent systems were collected. After implementing the basic models, the development of the ANFIS model was performed using the new supply–demand-based optimization (SDO) algorithm. This new model performed well compared to the base model. The SDO-ANFIS was also investigated against metaheuristic algorithms, PSO, ICA, and GA. In order to train the hybrid model, 48 pieces of data were considered. A total of 11 pieces of data were also used to test the model. According to the conducted analyses, the following items can be concluded:

- Among the 14 different combinations, the data that included six inputs had less errors;
- Using the model developed in this research and according to the six input parameters, an exact estimation of K_s can be obtained. The experimental data are the main source for the hybrid model training. The quality and quantity of these data thus directly affect the hybrid model performance. In fact, the hybrid model error reduces as the volume of data increases;

- The results of the ANFIS base model for the training and testing sections were R^2 = 0.8961 and 0.8821, respectively, and with the development of the model with the SDO algorithm, their accuracy increased to 0.9501 and 0.9449, respectively;
- The results show that the RMSE of hybrid models provide more appropriate values in predicting the K_s in comparison with the basic ANFIS. For the test results, the new SDO-ANFIS model obtained values of RMSE = 0.134, which performed better than other models. Therefore, the SDO-ANFIS model has higher accuracy and less error than other hybrid models for K_s prediction.

The best parameter that has the most impact on the K_s is the X2 (φ_h) parameter while X1 (m) was the least effective parameter. The methodology implemented in this research can be used for other engineering problems to identify influential parameters, find significant combinations of input data, and increase the performance of predictive models using optimization algorithms. New optimization algorithms, new machine learning models, and new datasets can be used for future research.

Author Contributions: Conceptualization, G.C., S.H.L. and A.S.A.R.; methodology, G.C., S.H.L. and A.S.A.R.; formal analysis, G.C., S.H.L. and A.S.A.R.; writing—original draft preparation, G.C., S.H.L., A.S.A.R., D.V.U. and B.W.; writing—review and editing, G.C., S.H.L., A.S.A.R., D.V.U. and B.W.; supervision, S.H.L. and A.S.A.R. All authors have read and agreed to the published version of the manuscript.

Funding: This research received no external funding.

Institutional Review Board Statement: Not applicable.

Informed Consent Statement: Not applicable.

Data Availability Statement: The data are available from the corresponding author upon reasonable request.

Acknowledgments: The authors would like to thank Universiti Teknologi Malaysia for the Fundamental Research grant with a reference number of Q.J130000.3851.21H90.

Conflicts of Interest: The authors declare no conflict of interest.

References

1. Vincevica-Gaile, Z.; Teppand, T.; Kriipsalu, M.; Krievans, M.; Jani, Y.; Klavins, M.; Hendroko Setyobudi, R.; Grinfelde, I.; Rudovica, V.; Tamm, T. Towards sustainable soil stabilization in peatlands: Secondary raw materials as an alternative. *Sustainability* **2021**, *13*, 6726. [CrossRef]
2. Kent, D.C.; Park, R. Flexural members with confined concrete. *J. Struct. Div.* **1971**, *97*, 1969–1990. [CrossRef]
3. Park, R.; Priestley, M.J.; Gill, W.D. Ductility of square-confined concrete columns. *J. Struct. Div.* **1982**, *108*, 929–950. [CrossRef]
4. Sheikh, S.A.; Uzumeri, S.M. Analytical model for concrete confinement in tied columns. *J. Struct. Div.* **1982**, *108*, 2703–2722. [CrossRef]
5. Sheikh, S.A.; Uzumeri, S.M. Strength and ductility of tied concrete columns. *J. Struct. Div.* **1980**, *106*, 1079–1102. [CrossRef]
6. Saatcioglu, M.; Razvi, S.R. Strength and ductility of confined concrete. *J. Struct. Eng.* **1992**, *118*, 1590–1607. [CrossRef]
7. Razvi, S.; Saatcioglu, M. Confinement model for high-strength concrete. *J. Struct. Eng.* **1999**, *125*, 281–289. [CrossRef]
8. Chung, H.-S.; Yang, K.-H.; Lee, Y.-H.; Eun, H.-C. Stress–strain curve of laterally confined concrete. *Eng. Struct.* **2002**, *24*, 1153–1163. [CrossRef]
9. Flood, I. A neural network approach to the sequencing of construction tasks. In Proceedings of the Proceedings of the Sixth International Symposium on Automation and Robotics in Construction, Construction Industry Institute, San Francisco, CA, USA, 6–8 June 1989.
10. Ren, L.; Zhao, Z. An optimal neural network and concrete strength modeling. *Adv. Eng. Softw.* **2002**, *33*, 117–130. [CrossRef]
11. Cladera, A.; Marí, A.R. Shear design procedure for reinforced normal and high-strength concrete beams using artificial neural networks. Part I: Beams without stirrups. *Eng. Struct.* **2004**, *26*, 917–926. [CrossRef]
12. Naeej, M.; Bali, M.; Naeej, M.R.; Amiri, J.V. Prediction of lateral confinement coefficient in reinforced concrete columns using M5′ machine learning method. *KSCE J. Civ. Eng.* **2013**, *17*, 1714–1719. [CrossRef]
13. Yetilmezsoy, K.; Sihag, P.; Kıyan, E.; Doran, B. A benchmark comparison and optimization of Gaussian process regression, support vector machines, and M5P tree model in approximation of the lateral confinement coefficient for CFRP-wrapped rectangular/square RC columns. *Eng. Struct.* **2021**, *246*, 113106. [CrossRef]

14. Alacalı, S.N.; Akbaş, B.; Doran, B. Prediction of lateral confinement coefficient in reinforced concrete columns using neural network simulation. *Appl. Soft Comput.* **2011**, *11*, 2645–2655. [CrossRef]
15. Koopialipoor, M.; Fahimifar, A.; Ghaleini, E.N.; Momenzadeh, M.; Armaghani, D.J. Development of a new hybrid ANN for solving a geotechnical problem related to tunnel boring machine performance. *Eng. Comput.* **2020**, *36*, 345–357. [CrossRef]
16. Koopialipoor, M.; Ghaleini, E.N.; Tootoonchi, H.; Jahed Armaghani, D.; Haghighi, M.; Hedayat, A. Developing a new intelligent technique to predict overbreak in tunnels using an artificial bee colony-based ANN. *Environ. Earth Sci.* **2019**, *78*, 165. [CrossRef]
17. Zhou, J.; Guo, H.; Koopialipoor, M.; Armaghani, D.J.; Tahir, M.M. Investigating the effective parameters on the risk levels of rockburst phenomena by developing a hybrid heuristic algorithm. *Eng. Comput.* **2021**, *37*, 1679–1694. [CrossRef]
18. Yang, H.; Koopialipoor, M.; Armaghani, D.J.; Gordan, B.; Khorami, M.; Tahir, M.M. Intelligent design of retaining wall structures under dynamic conditions. *STEEL Compos. Struct.* **2019**, *31*, 629–640.
19. Mohamad, E.T.; Koopialipoor, M.; Murlidhar, B.R.; Rashiddel, A.; Hedayat, A.; Armaghani, D.J. A new hybrid method for predicting ripping production in different weathering zones through in-situ tests. *Measurement* **2019**, *147*, 106826. [CrossRef]
20. Sharbati, R.; Khoshnoudian, F.; Koopialipoor, M.; Tahir, M.M. Applying dual-tree complex discrete wavelet transform and gamma modulating function for simulation of ground motions. *Eng. Comput.* **2021**, *37*, 1519–1535. [CrossRef]
21. Zhou, J.; Li, C.; Koopialipoor, M.; Jahed Armaghani, D.; Thai Pham, B. Development of a new methodology for estimating the amount of PPV in surface mines based on prediction and probabilistic models (GEP-MC). *Int. J. Min. Reclam. Environ.* **2021**, *35*, 48–68. [CrossRef]
22. Mahdiyar, A.; Jahed Armaghani, D.; Koopialipoor, M.; Hedayat, A.; Abdullah, A.; Yahya, K. Practical Risk Assessment of Ground Vibrations Resulting from Blasting, Using Gene Expression Programming and Monte Carlo Simulation Techniques. *Appl. Sci.* **2020**, *10*, 472. [CrossRef]
23. Koopialipoor, M.; Tootoonchi, H.; Jahed Armaghani, D.; Tonnizam Mohamad, E.; Hedayat, A. Application of deep neural networks in predicting the penetration rate of tunnel boring machines. *Bull. Eng. Geol. Environ.* **2019**, *78*, 6347–6360. [CrossRef]
24. Tang, D.; Gordan, B.; Koopialipoor, M.; Jahed Armaghani, D.; Tarinejad, R.; Thai Pham, B.; Huynh, V. Van Seepage Analysis in Short Embankments Using Developing a Metaheuristic Method Based on Governing Equations. *Appl. Sci.* **2020**, *10*, 1761. [CrossRef]
25. Xu, C.; Gordan, B.; Koopialipoor, M.; Armaghani, D.J.; Tahir, M.M.; Zhang, X. Improving Performance of Retaining Walls Under Dynamic Conditions Developing an Optimized ANN Based on Ant Colony Optimization Technique. *IEEE Access* **2019**, *7*, 94692–94700. [CrossRef]
26. Asteris, P.G.; Plevris, V. Anisotropic masonry failure criterion using artificial neural networks. *Neural Comput. Appl.* **2017**, *28*, 2207–2229. [CrossRef]
27. Zhang, H.; Nguyen, H.; Bui, X.-N.; Pradhan, B.; Asteris, P.G.; Costache, R.; Aryal, J. A generalized artificial intelligence model for estimating the friction angle of clays in evaluating slope stability using a deep neural network and Harris Hawks optimization algorithm. *Eng. Comput.* **2022**, *38*, 3901–3914. [CrossRef]
28. Bokolo, A.J. Green campus paradigms for sustainability attainment in higher education institutions—A comparative study. *J. Sci. Technol. Policy Manag.* **2020**, *12*, 117–148.
29. Shirkhani, A.; Davarnia, D.; Azar, B.F. Prediction of bond strength between concrete and rebar under corrosion using ANN. *Comput. Concr.* **2019**, *23*, 273–279.
30. Liu, Z.; Armaghani, D.J.; Fakharian, P.; Li, D.; Ulrikh, D.V.; Orekhova, N.N.; Khedher, K.M. Rock Strength Estimation Using Several Tree-Based ML Techniques. *C. Model. Eng. Sci.* **2022**, *133*, 799–824. [CrossRef]
31. Asteris, P.G.; Rizal, F.I.M.; Koopialipoor, M.; Roussis, P.C.; Ferentinou, M.; Armaghani, D.J.; Gordan, B. Slope Stability Classification under Seismic Conditions Using Several Tree-Based Intelligent Techniques. *Appl. Sci.* **2022**, *12*, 1753. [CrossRef]
32. Asteris, P.G.; Lourenço, P.B.; Roussis, P.C.; Adami, C.E.; Armaghani, D.J.; Cavaleri, L.; Chalioris, C.E.; Hajihassani, M.; Lemonis, M.E.; Mohammed, A.S. Revealing the nature of metakaolin-based concrete materials using artificial intelligence techniques. *Constr. Build. Mater.* **2022**, *322*, 126500. [CrossRef]
33. Armaghani, D.J.; Harandizadeh, H.; Momeni, E.; Maizir, H.; Zhou, J. *An Optimized System of GMDH-ANFIS Predictive Model by ICA for Estimating Pile Bearing Capacity*; Springer: Dodrecht, The Netherlands, 2022; Volume 55, ISBN 0123456789.
34. Shan, F.; He, X.; Armaghani, D.J.; Zhang, P.; Sheng, D. Success and challenges in predicting TBM penetration rate using recurrent neural networks. *Tunn. Undergr. Sp. Technol.* **2022**, *130*, 104728. [CrossRef]
35. Mahmood, W.; Mohammed, A.S.; Asteris, P.G.; Kurda, R.; Armaghani, D.J. Modeling Flexural and Compressive Strengths Behaviour of Cement-Grouted Sands Modified with Water Reducer Polymer. *Appl. Sci.* **2022**, *12*, 1016. [CrossRef]
36. Hasanipanah, M.; Monjezi, M.; Shahnazar, A.; Armaghani, D.J.; Farazmand, A. Feasibility of indirect determination of blast induced ground vibration based on support vector machine. *Measurement* **2015**, *75*, 289–297. [CrossRef]
37. Chen, L.; Asteris, P.G.; Tsoukalas, M.Z.; Armaghani, D.J.; Ulrikh, D.V.; Yari, M. Forecast of Airblast Vibrations Induced by Blasting Using Support Vector Regression Optimized by the Grasshopper Optimization (SVR-GO) Technique. *Appl. Sci.* **2022**, *12*, 9805. [CrossRef]
38. Barkhordari, M.; Armaghani, D.; Asteris, P. Structural Damage Identification Using Ensemble Deep Convolutional Neural Network Models. *C. Model. Eng. Sci.* **2023**, *134*, 835–855. [CrossRef]

39. Kardani, N.; Bardhan, A.; Samui, P.; Nazem, M.; Asteris, P.G.; Zhou, A. Predicting the thermal conductivity of soils using integrated approach of ANN and PSO with adaptive and time-varying acceleration coefficients. *Int. J. Therm. Sci.* **2022**, *173*, 107427. [CrossRef]
40. Koopialipoor, M.; Asteris, P.G.; Mohammed, A.S.; Alexakis, D.E.; Mamou, A.; Armaghani, D.J. Introducing stacking machine learning approaches for the prediction of rock deformation. *Transp. Geotech.* **2022**, *34*, 100756. [CrossRef]
41. Parsajoo, M.; Armaghani, D.J.; Mohammed, A.S.; Khari, M.; Jahandari, S. Tensile strength prediction of rock material using non-destructive tests: A comparative intelligent study. *Transp. Geotech.* **2021**, *31*, 100652. [CrossRef]
42. Asteris, P.G.; Mamou, A.; Hajihassani, M.; Hasanipanah, M.; Koopialipoor, M.; Le, T.-T.; Kardani, N.; Armaghani, D.J. Soft computing based closed form equations correlating L and N-type Schmidt hammer rebound numbers of rocks. *Transp. Geotech.* **2021**, *29*, 100588. [CrossRef]
43. Skentou, A.D.; Bardhan, A.; Mamou, A.; Lemonis, M.E.; Kumar, G.; Samui, P.; Armaghani, D.J.; Asteris, P.G. Closed-Form Equation for Estimating Unconfined Compressive Strength of Granite from Three Non-destructive Tests Using Soft Computing Models. *Rock Mech. Rock Eng.* **2022**. [CrossRef]
44. Ghanizadeh, A.R.; Ghanizadeh, A.; Asteris, P.G.; Fakharian, P.; Armaghani, D.J. Developing Bearing Capacity Model for Geogrid-Reinforced Stone Columns Improved Soft Clay utilizing MARS-EBS Hybrid Method. *Transp. Geotech.* **2023**, *38*, 100906. [CrossRef]
45. Indraratna, B.; Armaghani, D.J.; Correia, A.G.; Hunt, H.; Ngo, T. Prediction of resilient modulus of ballast under cyclic loading using machine learning techniques. *Transp. Geotech.* **2023**, *38*, 100895. [CrossRef]
46. Cavaleri, L.; Barkhordari, M.S.; Repapis, C.C.; Armaghani, D.J.; Ulrikh, D.V.; Asteris, P.G. Convolution-based ensemble learning algorithms to estimate the bond strength of the corroded reinforced concrete. *Constr. Build. Mater.* **2022**, *359*, 129504. [CrossRef]
47. Koopialipoor, M.; Fallah, A.; Armaghani, D.J.; Azizi, A.; Mohamad, E.T. Three hybrid intelligent models in estimating flyrock distance resulting from blasting. *Eng. Comput.* **2019**, *35*, 243–256. [CrossRef]
48. Koopialipoor, M.; Noorbakhsh, A.; Noroozi Ghaleini, E.; Jahed Armaghani, D.; Yagiz, S. A new approach for estimation of rock brittleness based on non-destructive tests. *Nondestruct. Test. Eval.* **2019**, *34*, 354–375. [CrossRef]
49. Yang, H.; Song, K.; Zhou, J. Automated Recognition Model of Geomechanical Information Based on Operational Data of Tunneling Boring Machines. *Rock Mech. Rock Eng.* **2022**, *55*, 1499–1516. [CrossRef]
50. Yang, H.; Wang, Z.; Song, K. A new hybrid grey wolf optimizer-feature weighted-multiple kernel-support vector regression technique to predict TBM performance. *Eng. Comput.* **2022**, *38*, 2469–2485. [CrossRef]
51. Yang, H.Q.; Li, Z.; Jie, T.Q.; Zhang, Z.Q. Effects of joints on the cutting behavior of disc cutter running on the jointed rock mass. *Tunn. Undergr. Sp. Technol.* **2018**, *81*, 112–120. [CrossRef]
52. Yang, H.; Wang, H.; Zhou, X. Analysis on the damage behavior of mixed ground during TBM cutting process. *Tunn. Undergr. Sp. Technol.* **2016**, *57*, 55–65. [CrossRef]
53. Ghanizadeh, A.R.; Delaram, A.; Fakharian, P.; Armaghani, D.J. Developing Predictive Models of Collapse Settlement and Coefficient of Stress Release of Sandy-Gravel Soil via Evolutionary Polynomial Regression. *Appl. Sci.* **2022**, *12*, 9986. [CrossRef]
54. Li, C.; Zhou, J.; Tao, M.; Du, K.; Wang, S.; Armaghani, D.J.; Mohamad, E.T. Developing hybrid ELM-ALO, ELM-LSO and ELM-SOA models for predicting advance rate of TBM. *Transp. Geotech.* **2022**, *36*, 100819. [CrossRef]
55. Armaghani, D.J.; Koopialipoor, M.; Marto, A.; Yagiz, S. Application of several optimization techniques for estimating TBM advance rate in granitic rocks. *J. Rock Mech. Geotech. Eng.* **2019**, *11*, 779–789. [CrossRef]
56. Sun, L.; Koopialipoor, M.; Armaghani, D.J.; Tarinejad, R.; Tahir, M.M. Applying a meta-heuristic algorithm to predict and optimize compressive strength of concrete samples. *Eng. Comput.* **2021**, *37*, 1133–1145. [CrossRef]
57. Koopialipoor, M.; Armaghani, D.J.; Hedayat, A.; Marto, A.; Gordan, B. Applying various hybrid intelligent systems to evaluate and predict slope stability under static and dynamic conditions. *Soft Comput.* **2019**, *23*, 5913–5929. [CrossRef]
58. Papadimitropoulos, V.C.; Tsikas, P.K.; Chassiakos, A.P. Modeling the Influence of Environmental Factors on Concrete Evaporation Rate. *J. Soft Comput. Civ. Eng.* **2020**, *4*, 79–97.
59. Erzin, Y.; MolaAbasi, H.; Kordnaeij, A.; Erzin, S. Prediction of Compression Index of Saturated Clays Using Robust Optimization Model. *J. Soft Comput. Civ. Eng.* **2020**, *4*, 1–16.
60. Teimouri, F.; Ghatee, M. A Real-Time Warning System for Rear-End Collision Based on Random Forest Classifier. *J. Soft Comput. Civ. Eng.* **2020**, *4*, 49–71.
61. Ikram, R.M.A.; Dai, H.-L.; Ewees, A.A.; Shiri, J.; Kisi, O.; Zounemat-Kermani, M. Application of improved version of multi verse optimizer algorithm for modeling solar radiation. *Energy Rep.* **2022**, *8*, 12063–12080. [CrossRef]
62. Adnan, R.M.; Ewees, A.A.; Parmar, K.S.; Yaseen, Z.M.; Shahid, S.; Kisi, O. The viability of extended marine predators algorithm-based artificial neural networks for streamflow prediction. *Appl. Soft Comput.* **2022**, *131*, 109739.
63. Rafiq, M.Y.; Bugmann, G.; Easterbrook, D.J. Neural network design for engineering applications. *Comput. Struct.* **2001**, *79*, 1541–1552. [CrossRef]
64. Park, R.; Paulay, T. *Reinforced Concrete Structures*; John Wiley & Sons: Hoboken, NJ, USA, 1975; ISBN 0471659177.
65. Ezekiel, M. The cobweb theorem. *Q. J. Econ.* **1938**, *52*, 255–280. [CrossRef]
66. Zhao, W.; Wang, L.; Zhang, Z. Supply-demand-based optimization: A novel economics-inspired algorithm for global optimization. *IEEE Access* **2019**, *7*, 73182–73206. [CrossRef]

67. Han, T.H.; Lim, N.H.; Han, S.Y.; Park, J.S.; Kang, Y.J. Nonlinear concrete model for an internally confined hollow reinforced concrete column. *Mag. Concr. Res.* **2008**, *60*, 429–440. [CrossRef]
68. Samani, A.K.; Attard, M.M. A stress–strain model for uniaxial and confined concrete under compression. *Eng. Struct.* **2012**, *41*, 335–349. [CrossRef]
69. Isleem, H.F.; Tayeh, B.A.; Alaloul, W.S.; Musarat, M.A.; Raza, A. Artificial neural network (ANN) and finite element (FEM) models for GFRP-reinforced concrete columns under axial compression. *Materials* **2021**, *14*, 7172. [CrossRef] [PubMed]
70. Yurdakul, M.; Gopalakrishnan, K.; Akdas, H. Prediction of specific cutting energy in natural stone cutting processes using the neuro-fuzzy methodology. *Int. J. Rock Mech. Min. Sci.* **2014**, *67*, 127–135. [CrossRef]